Supporting information for Dilution impacts on smoke aging: Evidence in BBOP data

Text S1. BBOP instrumentation

The FIMS characterizes particle sizes based on electrical mobility as in scanning mobility particle sizer (SMPS). Because FIMS measures particles of different sizes simultaneously instead of sequentially as in traditional SMPS, it provides aerosol size distribution with a much higher time resolution at 1 Hz (Wang et al., 2017). The relative humidity of the aerosol sample was reduced to below ~25% using a Nafion dryer before being introduced into the FIMS. Therefore, the measured size distributions represented that of the dry aerosol particles.

An SPN1 radiometer (Badosa et al. 2014; Long et al. 2010) provided total shortwave irradiance, with a shaded mask applied following (Badosa et al. 2014). The data was corrected for tilt up to 10 degrees of tilt, following (Long et al. 2010). For tilt greater than 10 degrees these values are set to "bad".

References

Text S2. Heterogeneous chemistry calculations

We test the impact of heterogeneous chemistry on aerosol mass loss within the smoke plume. We performed a simple calculation of OH molecules collision to the surface of a single particle ranging from 1 nm to 1 μm size in diameter. The following parameters assumed for the calculations:

- OH diffusivity = 3.5e-5 [m2 s-1]
- Constant OH concentration varied from 1e5 to 5e7 [molecules cm-3]
- Molecular weight of organics = 200 [g mol-1]
- Density of organics = 1.4 [g cm-3]
- Total run time = 3 [hours]

As an upper bound calculation, we assume each collision results in removing an organic molecule on the surface of the particle (assumed to be 200 amu), fragmenting and removing the molecule from the particle. The fragmentation products are not assumed to participate in further reaction. Figure S23a shows the resulting final:initial mass ratios after four hours of aging, indicating that for all aerosol sizes captured in this study (>10 nm) and under a range of OH concentrations, >90% of the aerosol mass remains. As a lower bound, we also include a case in which only 10% of all OH collisions result in a mass loss of 200 amu (Figure S23c).(Slade and Knopf 2013)

Badosa, Jordi, John Wood, Philippe Blanc, Charles N. Long, Laurent Vuilleumier, Dominique Demengel, and Martial Haeffelin. 2014. “Solar Irradiances Measured Using SPN1 Radiometers: Uncertainties and Clues for Development.” *Atmospheric Measurement Techniques* 7: 4267–83.

Long, C. N., A. Bucholtz, H. Jonsson, B. Schmid, A. Vogelmann, and J. Wood. 2010. “A Method of Correcting for Tilt from Horizontal in Downwelling Shortwave Irradiance Measurements on Moving Platforms.” *The Open Atmospheric Science Journal*. https://doi.org/10.2174/1874282301004010078.

Slade, Jonathan H., and Daniel A. Knopf. 2013. “Heterogeneous OH Oxidation of Biomass Burning Organic Aerosol Surrogate Compounds: Assessment of Volatilisation Products and the Role of OH Concentration on the Reactive Uptake Kinetics.” *Physical Chemistry Chemical Physics: PCCP* 15 (16): 5898–5915.

Wang, J., Pikridas, M., Spielman, S. R., and Pinterich, T.: A fast integrated mobility spectrometer for rapid measurement of sub-micrometer aerosol size distribution, Part I: Design and model evaluation, J. Aerosol Sci., 108, 44-55, 10.1016/j.jaerosci.2017.02.012, 2017.

Table S1. Flight description table.

Flight name, date	Number of sets of pseudo-Lagrangian transects	Fire name	Fuel[1]	Missing data[2]
‘726a’, 07-26-2013	2	Mile Marker 28	grasslands, shrub brush, timber, and timber litter	
‘730a’, 07-30-2013	1	Colockum Tarps	grass, trees	
‘730b’, 07-30-2013	2	Colockum Tarps	grass, trees	
‘809a’, 08-09-2013	1	Colockum Tarps	grass, trees	NO_x
‘821b’, 08-21-2013	1	Government Flats		O_3

[1]When known
[2]Instruments relevant to this study

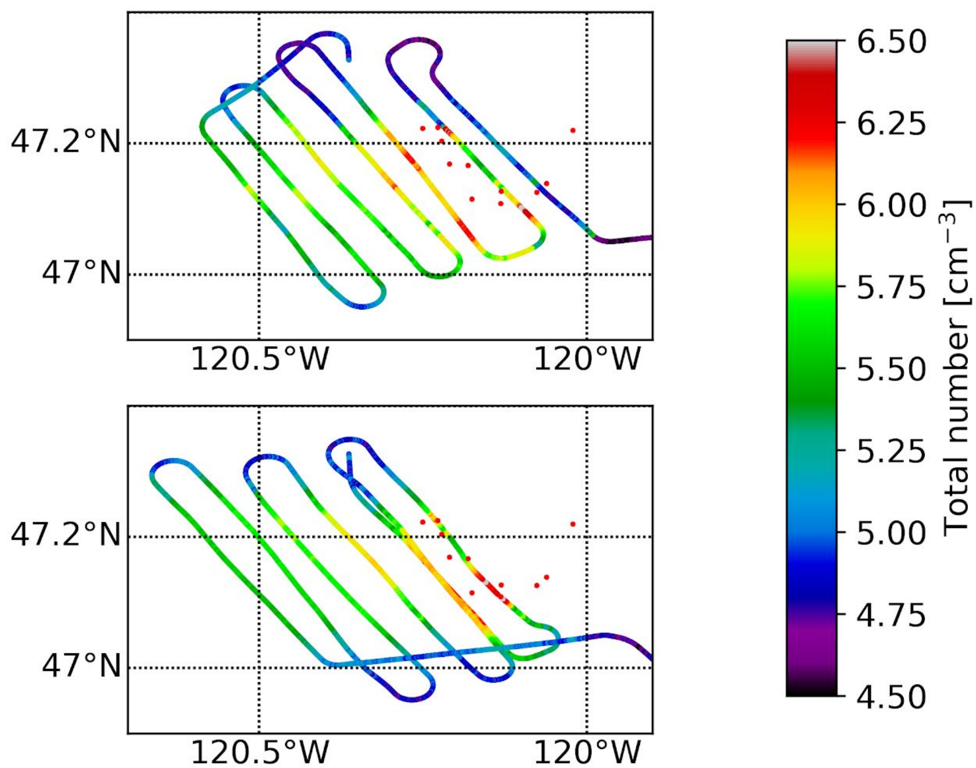

Figure S1. The flight path for flight '730b', colored by the FIMS total number concentration. The red dots are MODIS fire/thermal anomalies. The black star indicates the approximate center of the fire and the black dashed line indicates the approximate centerline of the plume, estimated by the number concentration. The numbers are the leg number.

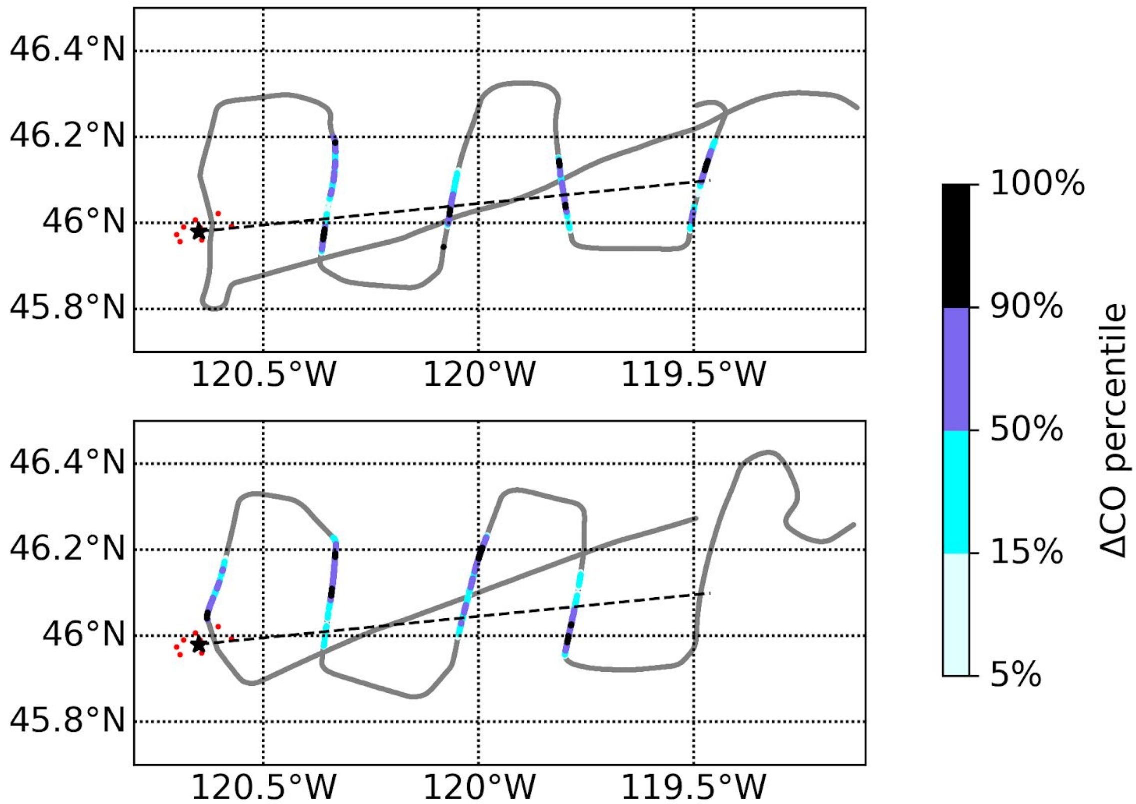

Figure S2. The flight path for ‘726a’. The legs used in this study are colored by each ΔCO percentile bin used in the main text analyses. There were two complete flight paths for this day. The red dots are MODIS fire/thermal anomalies. The black star indicates the approximate center of the fire and the black dashed line indicates the approximate centerline of the plume, estimated by the number concentration.

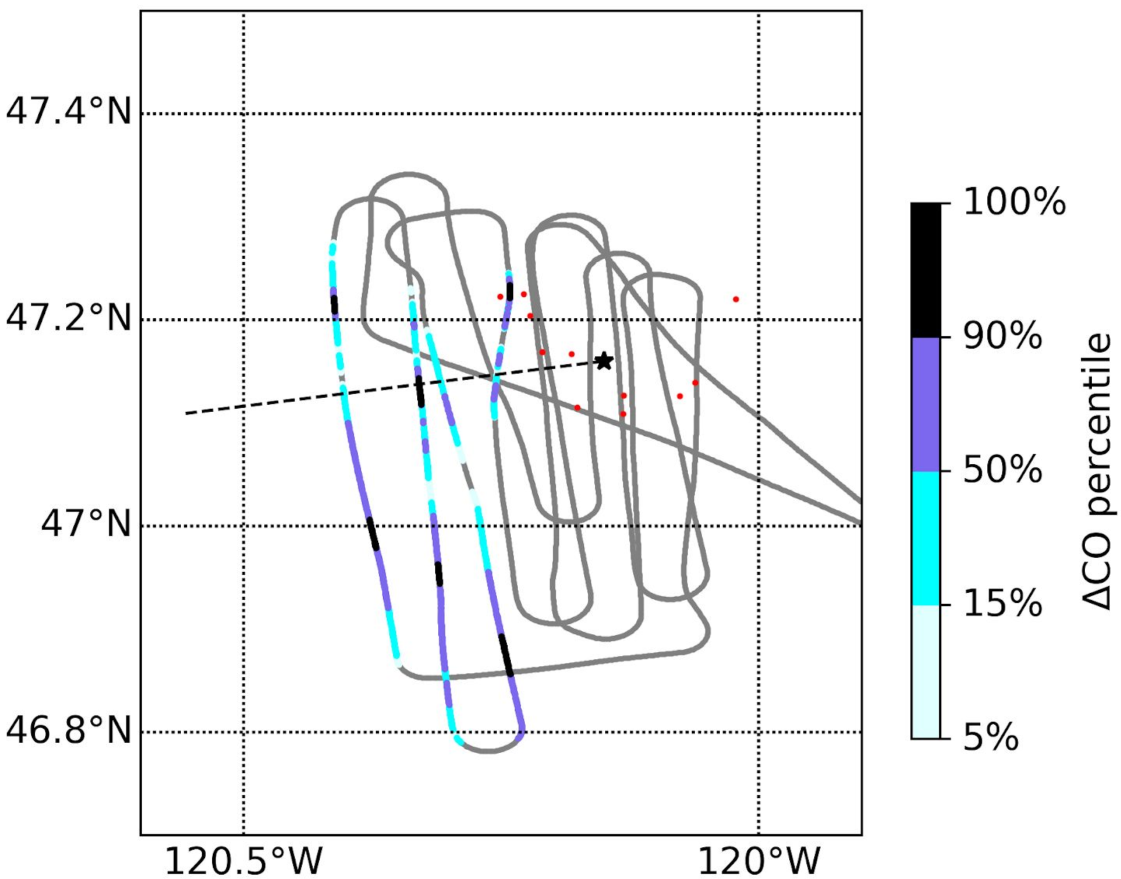

Figure S3. The flight path for '730a'. The legs used in this study are colored by each ΔCO percentile bin used in the main text analyses. The red dots are MODIS fire/thermal anomalies. The black star indicates the approximate center of the fire and the black dashed line indicates the approximate centerline of the plume, estimated by the number concentration.

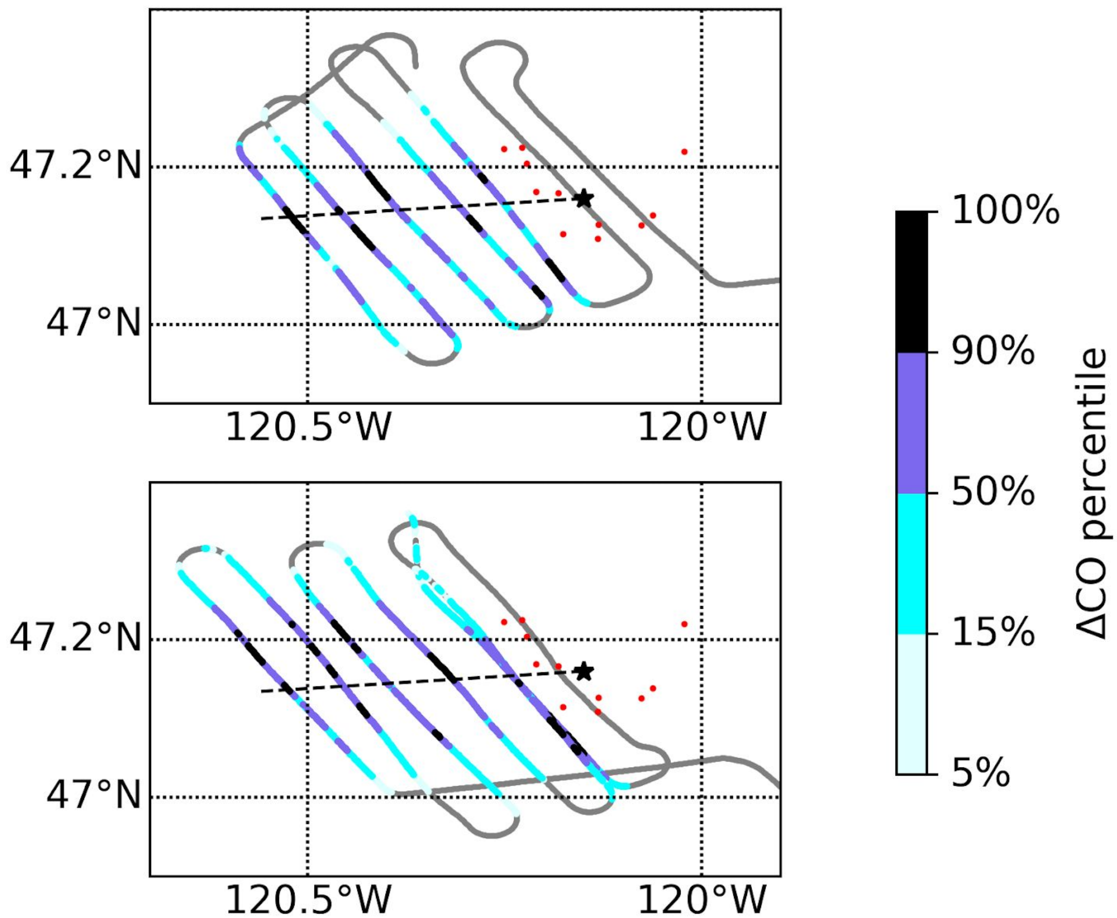

Figure S4. The flight path for ‘730b’. The legs used in this study are colored by each ΔCO percentile bin used in the main text analyses. There were two complete flight paths for this flight. The red dots are MODIS fire/thermal anomalies. The black star indicates the approximate center of the fire and the black dashed line indicates the approximate centerline of the plume, estimated by the number concentration.

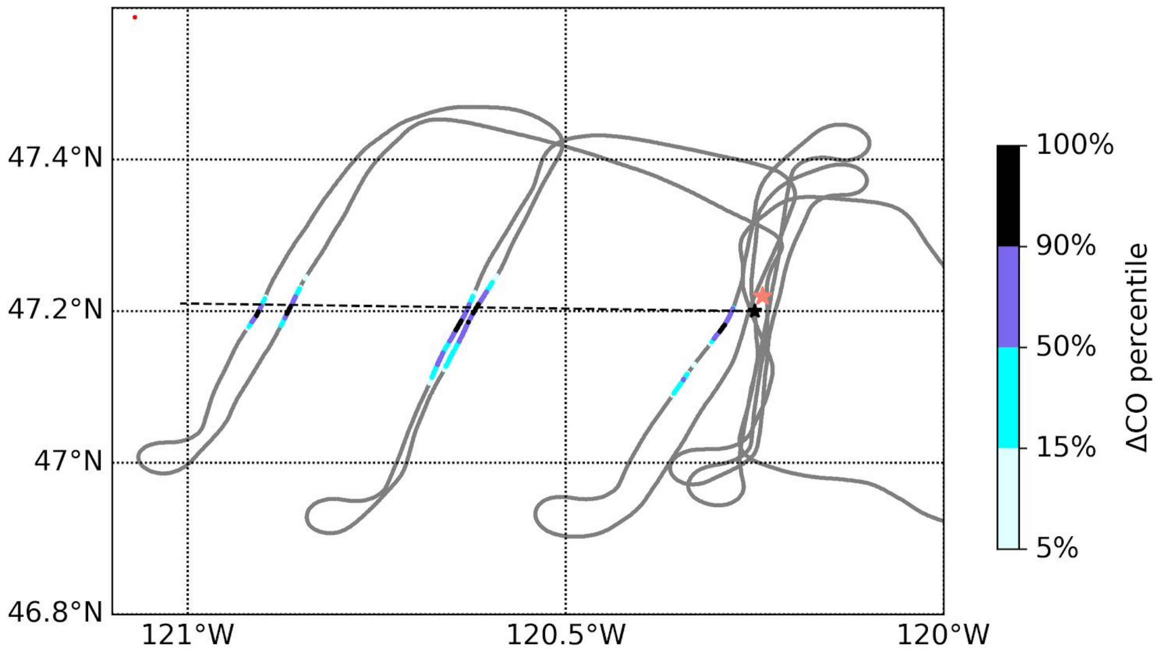

Figure S5. The flight path for '809a'. The legs used in this study are colored by each ΔCO percentile bin used in the main text analyses. The Worldview image for this day had clouds over the fire location at the time of the satellite passover. Thus we estimate a fire center using Worldview and MODIS images for this region on the previous day (8-08-2013) and the following day (8-10-2013) (salmon-colored star). The black star indicates the approximate center of the fire and the black dashed line indicates the approximate centerline of the plume, estimated by the number concentration.

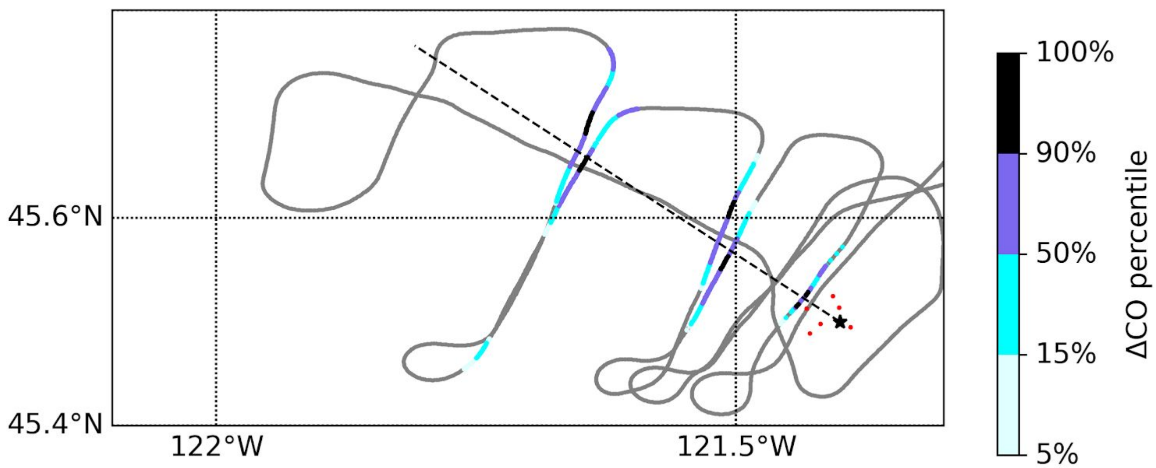

Figure S6. The flight path for ‘821b’. The legs used in this study are colored by each ΔCO percentile bin used in the main text analyses. The red dots are MODIS fire/thermal anomalies. The black star indicates the approximate center of the fire and the black dashed line indicates the approximate centerline of the plume, estimated by the number concentration.

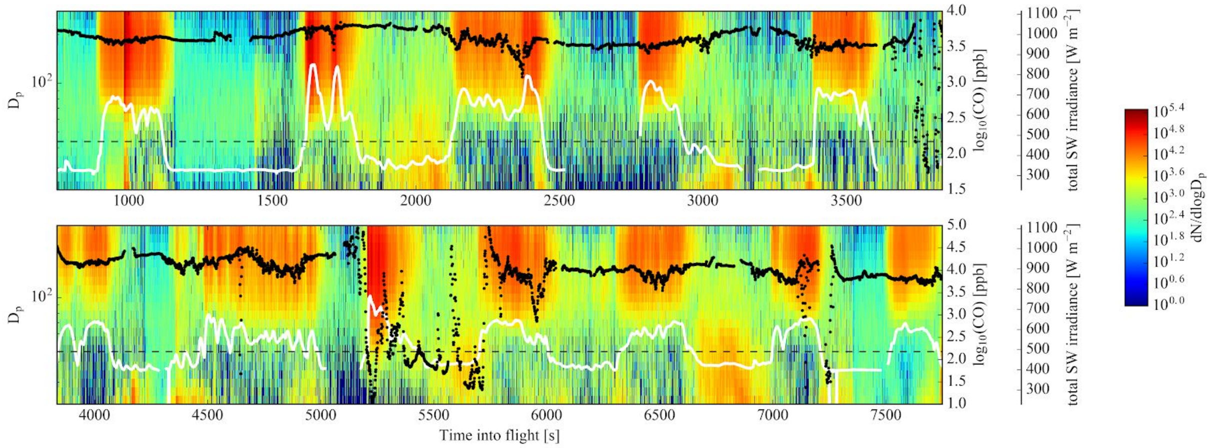

Figure S7. Number size distribution data, dN/dlogD$_p$, from the FIMS; CO (white solid line); and total short wave (SW) irradiance (black dots) data for the '726a' flight. The dotted dashed line indicates CO=150 ppb, our cutoff for in-plume/out-of-plume.

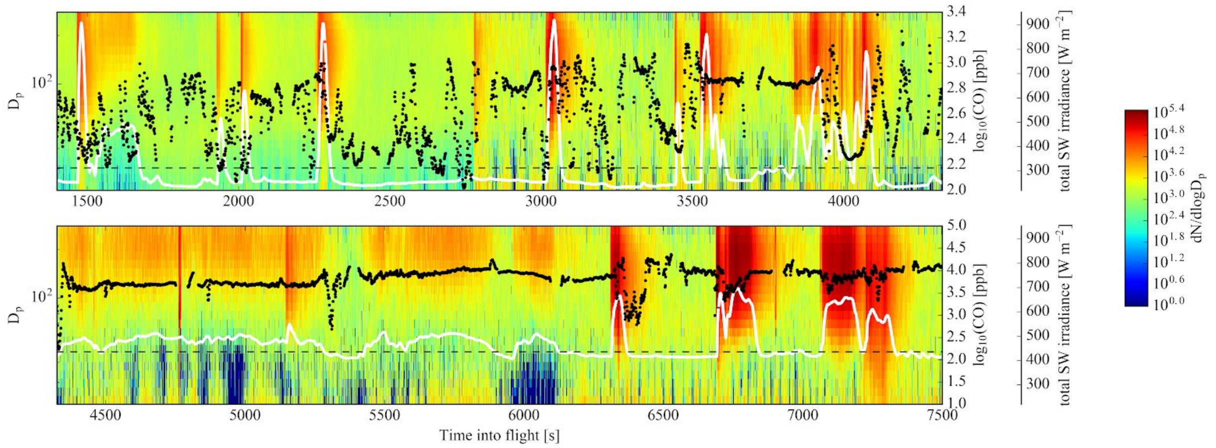

Figure S8. Number size distribution data, dN/dlogD_p, from the FIMS; CO (white solid line); and total short wave (SW) irradiance (black dots) data for the '730a' flight. The dotted dashed line indicates CO=150 ppb, our cutoff for in-plume/out-of-plume.

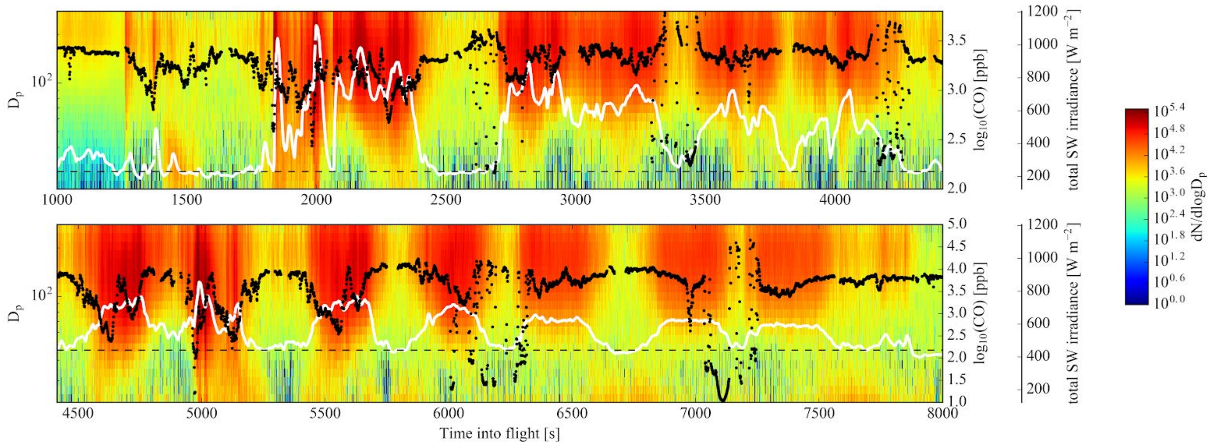

Figure S9. Number size distribution data, dN/dlogD$_p$, from the FIMS; CO (white solid line); and total short wave (SW) irradiance (black dots) data for the '730b' flight. The dotted dashed line indicates CO=150 ppb, our cutoff for in-plume/out-of-plume.

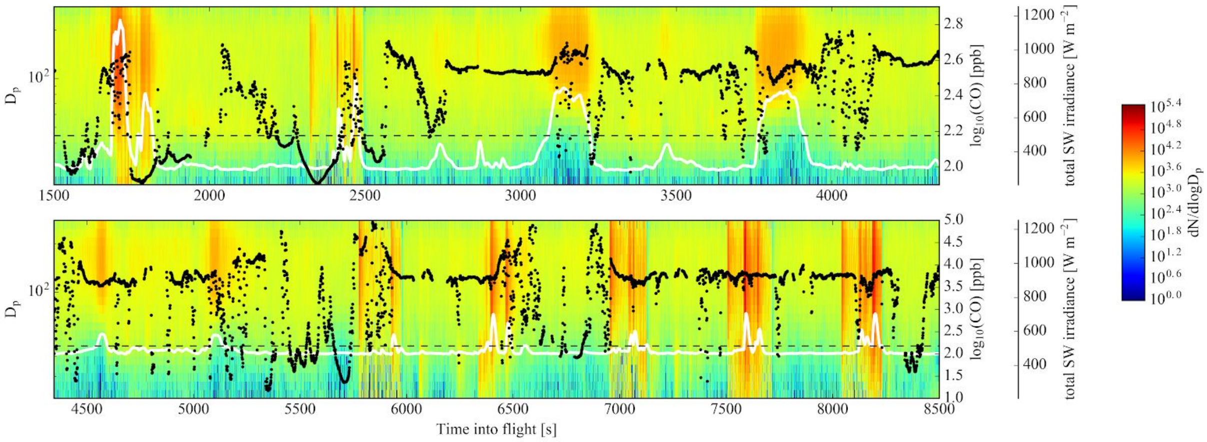

Figure S10. Number size distribution data, dN/dlogD_p, from the FIMS; CO (white solid line); and total short wave (SW) irradiance (black dots) data for the '809a' flight. The dotted dashed line indicates CO=150 ppb, our cutoff for in-plume/out-of-plume.

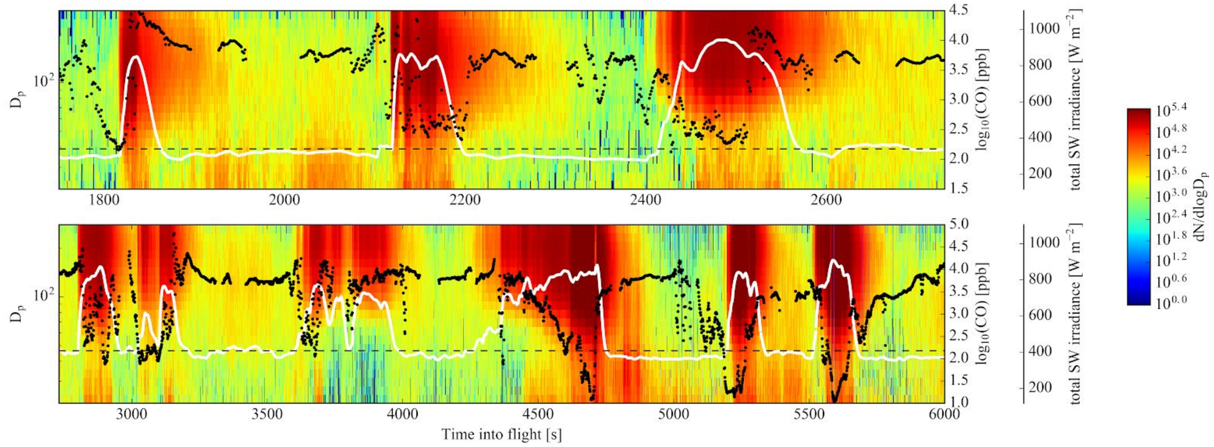

Figure S11. Number size distribution data, dN/dlogD$_p$, from the FIMS; CO (white solid line); and total short wave (SW) irradiance (black dots) data for the '821b' flight. The dotted dashed line indicates CO=150 ppb, our cutoff for in-plume/out-of-plume.

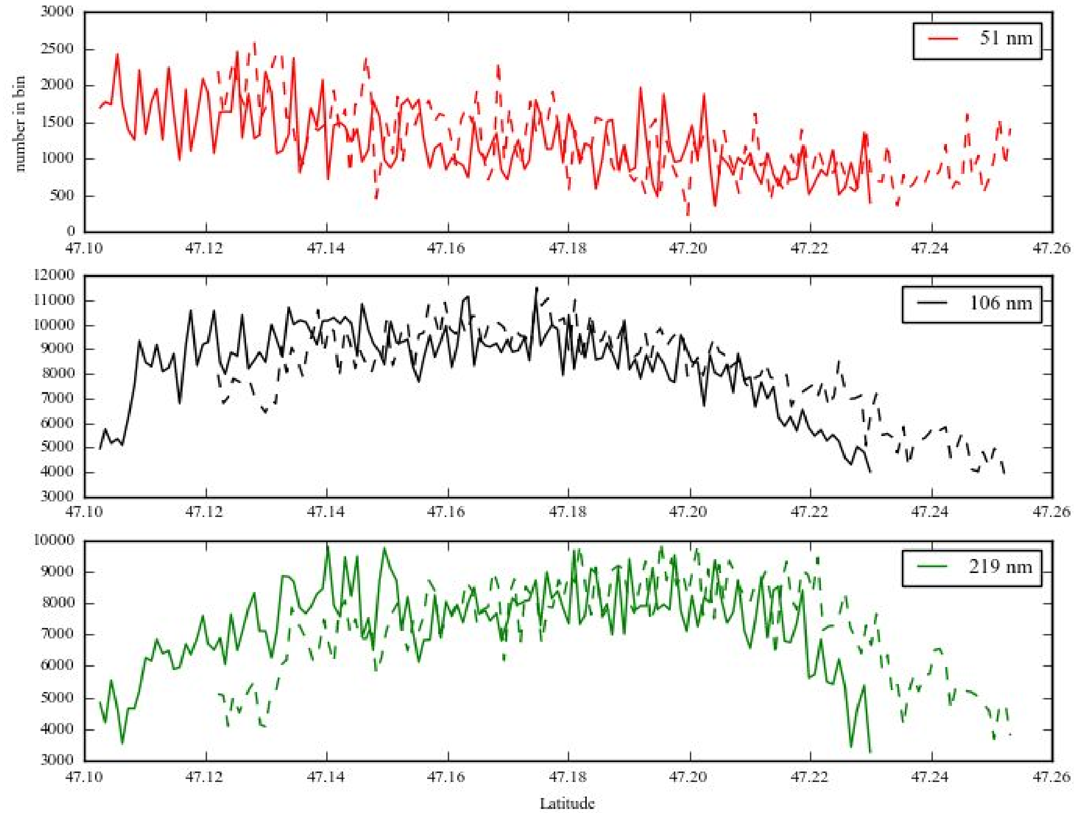

Figure S12. FIMS data for ‘809a’ for the two legs that ~overlap (Figure S5) for the 51, 106, and 219 nm size bins. The solid line is from the plane flying north to south (right to left in this figure) and the dashed line is from the plane flying south to north (left to right in this figure). In the absence of FIMS measurement artifacts, we expect these two lines to roughly match each other.

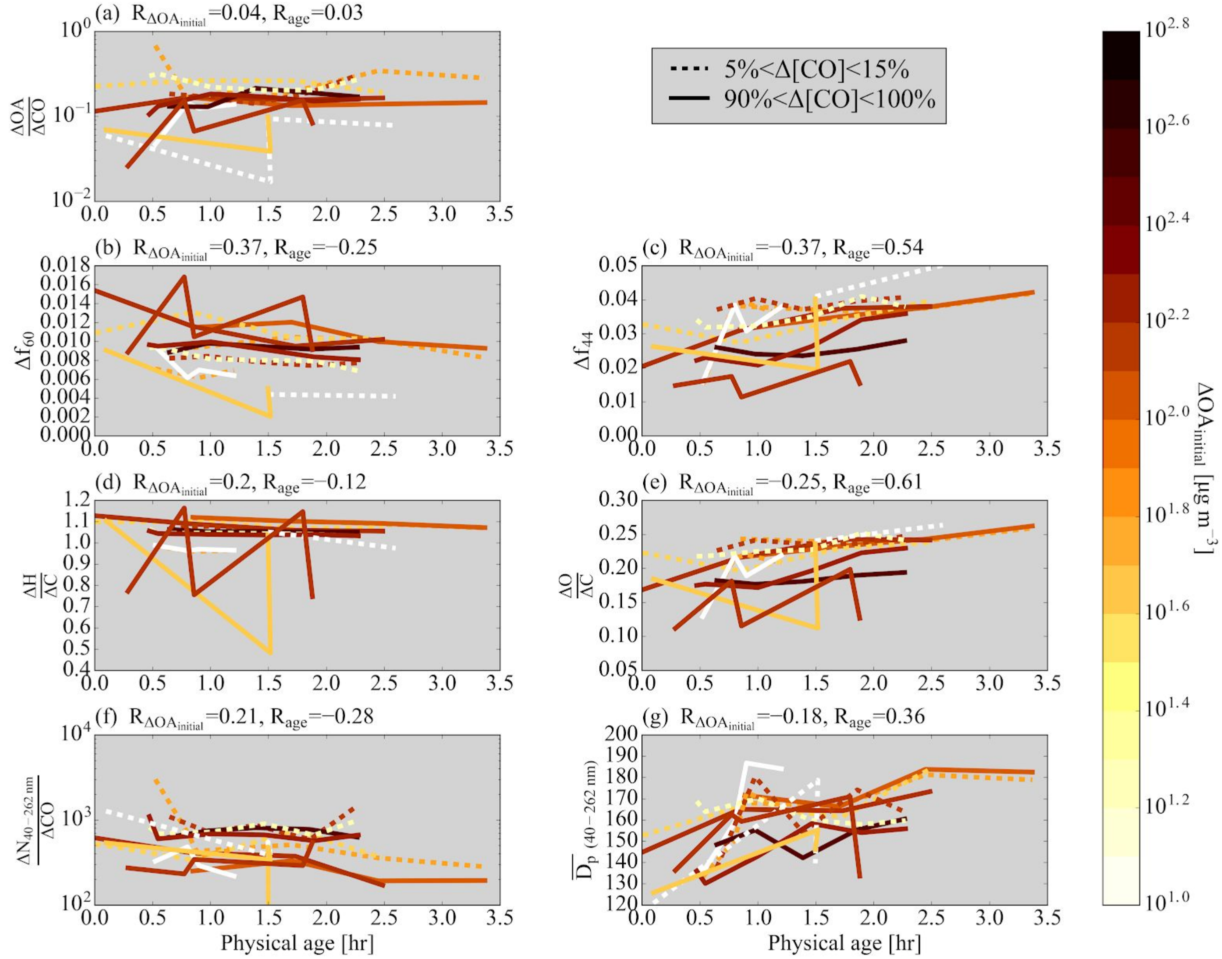

Figure S13. Same as Figure 2 but using only the first 50% of data for each leg of the FIMS and CO data for panels f-g.

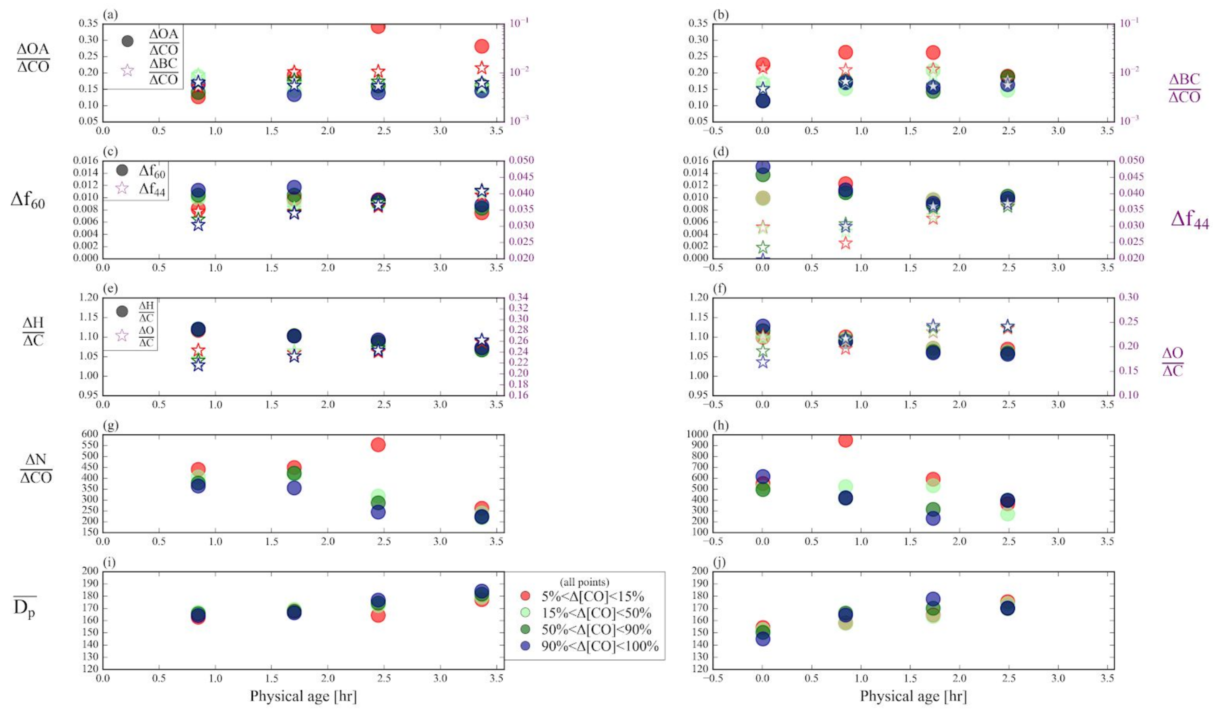

Figure S14. Aerosol properties for the first set (left-hand column) and second set (right-hand column) of pseudo-Lagrangian transects from flight '726a' (a-b) ΔOA/ΔCO (right y-axis) and ΔrBC/ΔCO (left y-axis), (c-d) Δf_{60} (right y-axis) and Δf_{44} (left y-axis), (e-f) ΔH/ΔC (right y-axis) and ΔO/ΔC (left y-axis), (g-h) ΔN/ΔCO, and (i-j) $\overline{D_p}$ against physical age. For each transect, the data is divided into edge (the lowest 5-15% of ΔCO data; red points), core (90-100% of ΔCO data; blue points), and intermediate regions (15-50% and 50-90% of ΔCO data; light green and dark green points). ΔrBC/ΔCO is shown in log scale and the x-axis for the right-hand column has been shifted backwards to improve clarity. Note that the left-hand and right-hand columns do not always have the same y-axis limits.

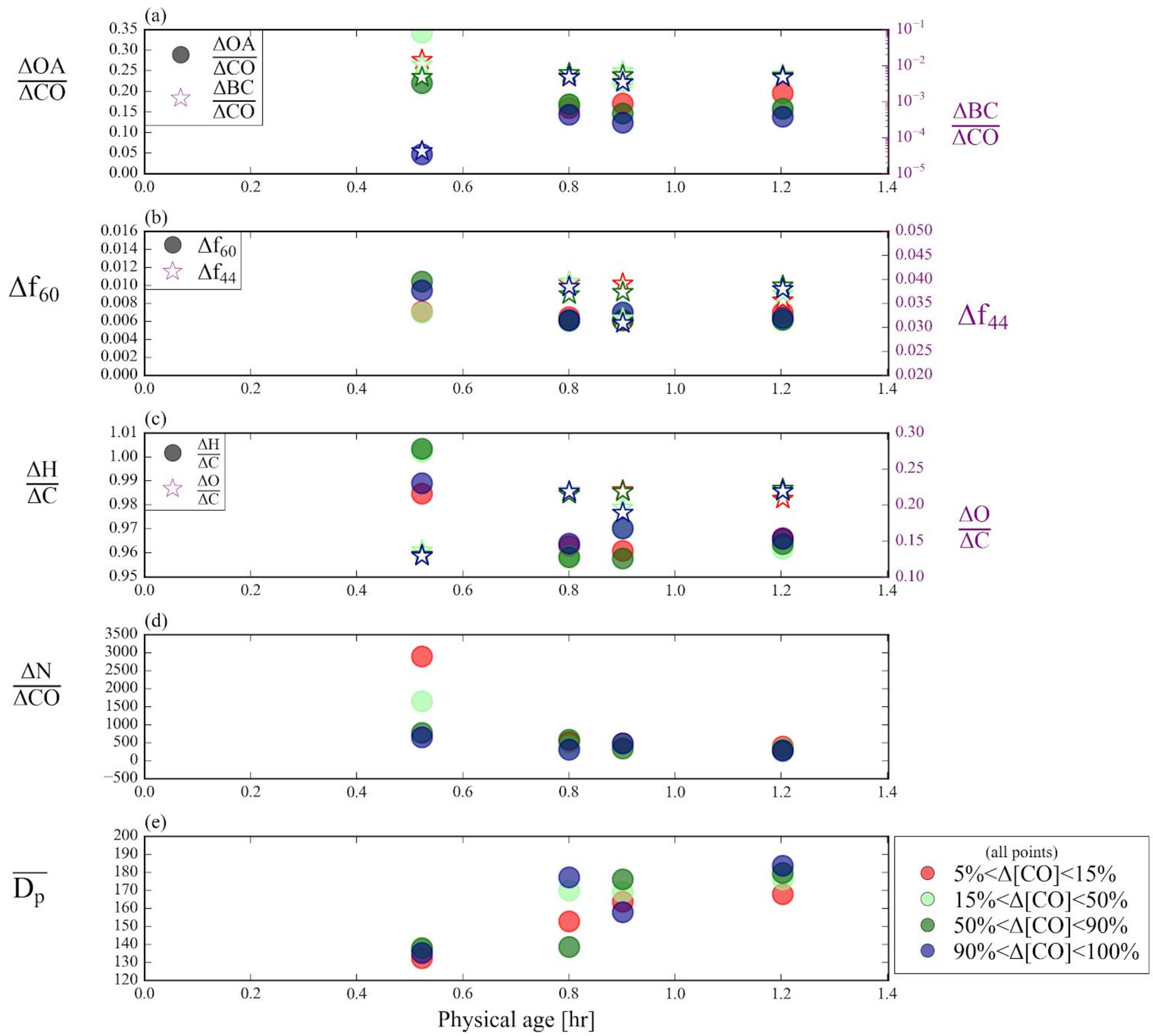

Figure S15. Aerosol properties for the set of pseudo-Lagrangian transects from flight '730a' (a) ΔOA/ΔCO (right y-axis) and ΔrBC/ΔCO (left y-axis), (b) Δf_{60} (right y-axis) and Δf_{44} (left y-axis), (c) ΔH/ΔC (right y-axis) and ΔO/ΔC (left y-axis), (d) ΔN/ΔCO, and (e) $\overline{D_p}$ against physical age. For each transect, the data is divided into edge (the lowest 5-15% of ΔCO data; red points), core (90-100% of ΔCO data; blue points), and intermediate regions (15-50% and 50-90% of ΔCO data; light green and dark green points). ΔrBC/ΔCO is shown in log scale to improve clarity.

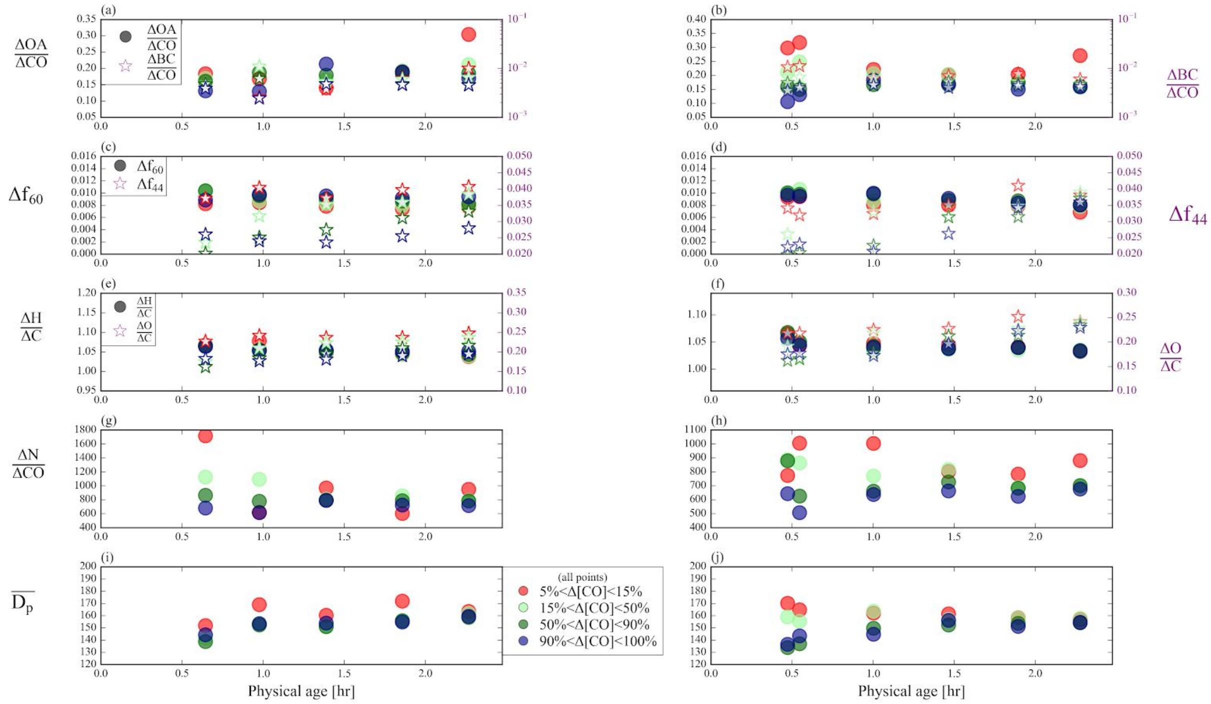

Figure S16. Aerosol properties for the first set (left-hand column) and second set (right-hand column) of pseudo-Lagrangian transects from flight '730b' (a-b) ΔOA/ΔCO (right y-axis) and ΔrBC/ΔCO (left y-axis), (c-d) Δf_{60} (right y-axis) and Δf_{44} (left y-axis), (e-f) ΔH/ΔC (right y-axis) and ΔO/ΔC (left y-axis), (g-h) ΔN/ΔCO, and (i-j) $\overline{D_p}$ against physical age. For each transect, the data is divided into edge (the lowest 5-15% of ΔCO data; red points), core (90-100% of ΔCO data; blue points), and intermediate regions (15-50% and 50-90% of ΔCO data; light green and dark green points). ΔrBC/ΔCO is shown in log scale to improve clarity. Note that the left-hand and right-hand columns do not always have the same y-axis limits.

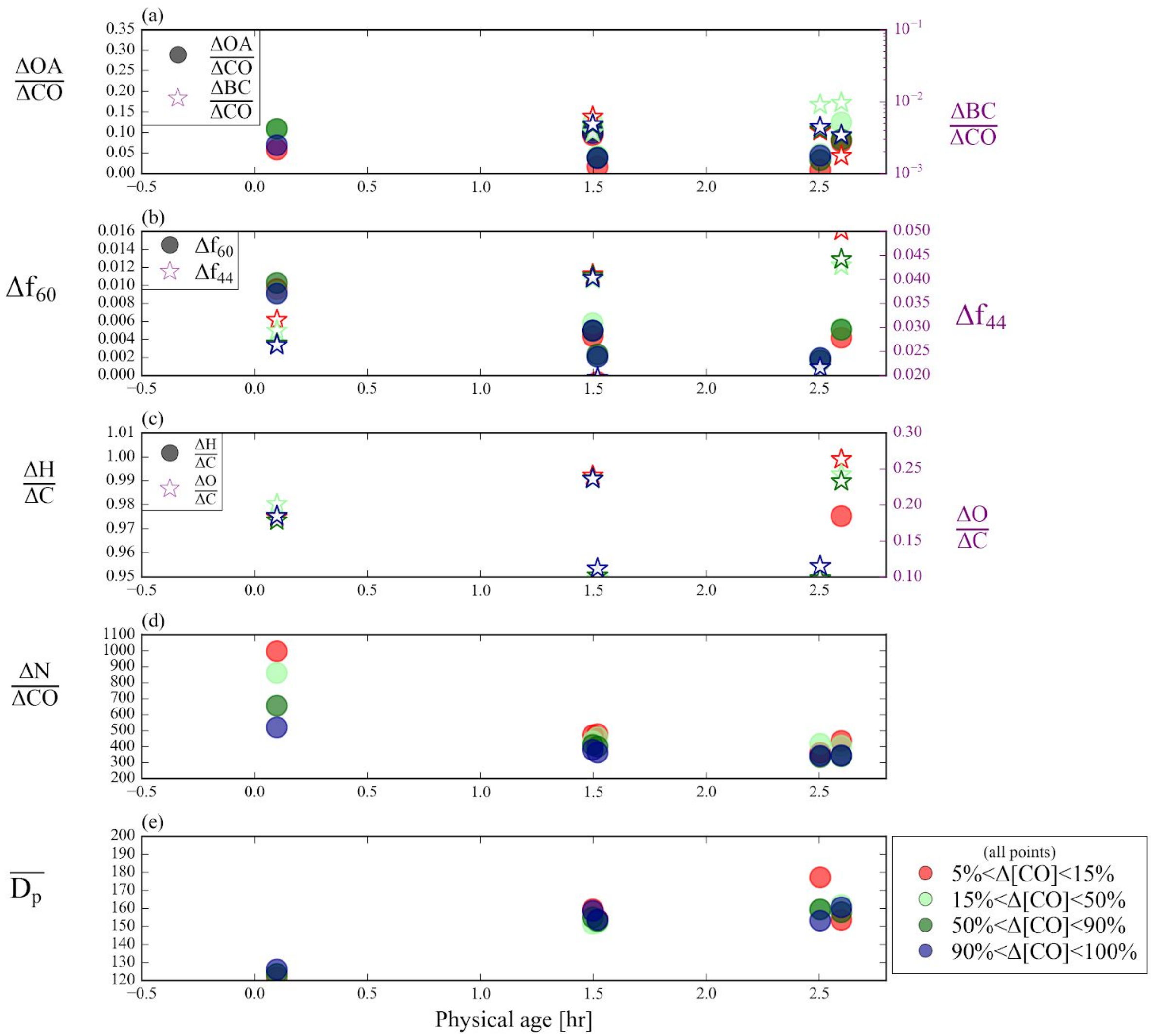

Figure S17. Aerosol properties for the set of pseudo-Lagrangian transects from flight '809a' (a) ΔOA/ΔCO (right y-axis) and ΔrBC/ΔCO (left y-axis), (b) Δf_{60} (right y-axis) and Δf_{44} (left y-axis), (c) ΔH/ΔC (right y-axis) and ΔO/ΔC (left y-axis), (d) ΔN/ΔCO, and (e) $\overline{D_p}$ against physical age. For each transect, the data is divided into edge (the lowest 5-15% of ΔCO data; red points), core (90-100% of ΔCO data; blue points), and intermediate regions (15-50% and 50-90% of ΔCO data; light green and dark green points). ΔrBC/ΔCO is shown in log scale and the x-axis for the right-hand column has been shifted backwards to improve clarity.

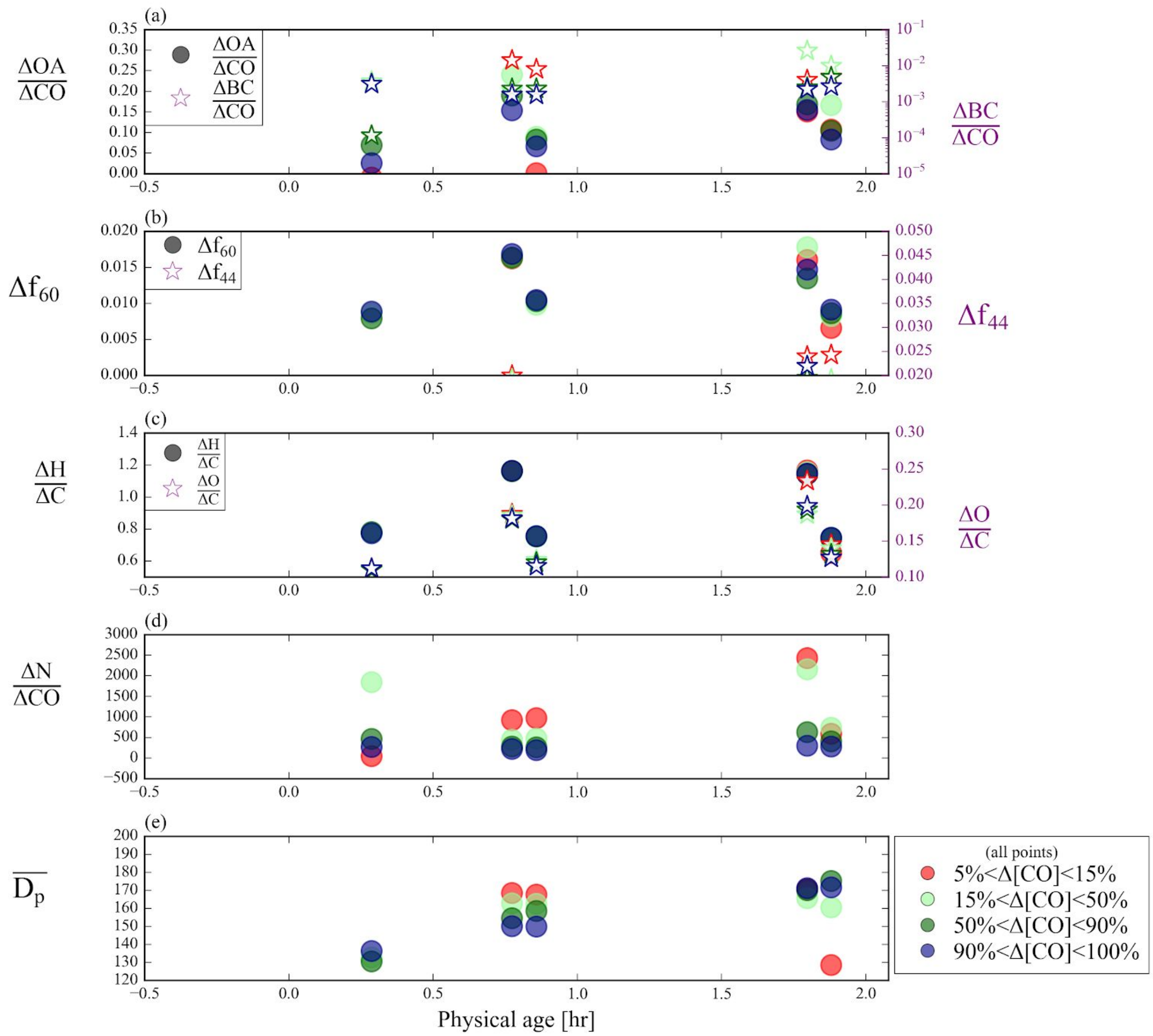

Figure S18. Aerosol properties for the set of pseudo-Lagrangian transects from flight '821b' (a) ΔOA/ΔCO (right y-axis) and ΔrBC/ΔCO (left y-axis), (b) Δf_{60} (right y-axis) and Δf_{44} (left y-axis), (c) ΔH/ΔC (right y-axis) and ΔO/ΔC (left y-axis), (d) ΔN/ΔCO, and (e) $\overline{D_p}$ against physical age. For each transect, the data is divided into edge (the lowest 5-15% of ΔCO data; red points), core (90-100% of ΔCO data; blue points), and intermediate regions (15-50% and 50-90% of ΔCO data; light green and dark green points). ΔrBC/ΔCO is shown in log scale and the x-axis for the right-hand column has been shifted backwards to improve clarity.

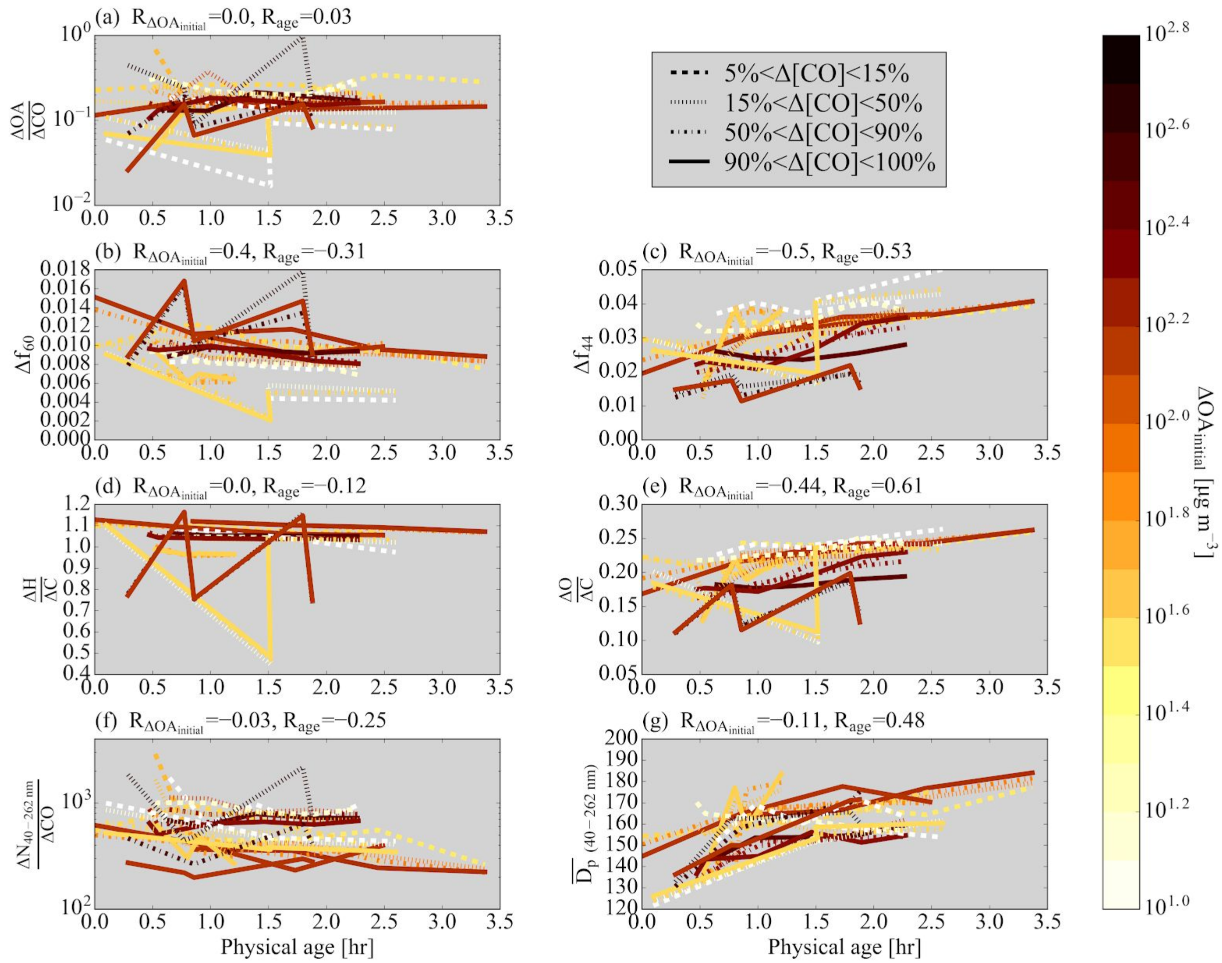

Figure S19. Various normalized parameters as a function of age for the 7 sets of pseudo-Lagrangian transects. Separate lines are shown for the edges (lowest 5-15% of ΔCO; dashed lines) cores (highest 90-100% of ΔCO; solid lines), and intermediate regions (15-50% and 50-90%; dotted and dashed-dot lines). (a) ΔOA/ΔCO, (b) Δf_{60}, (c) Δf_{44}, (d) ΔH/ΔC, (e) ΔO/ΔC, (f) $\Delta N_{40\text{-}262\ nm}$/ΔCO, and (g) $\overline{D_p}$ between 40-262 nm against physical age for all flights, colored by $\Delta OA_{initial}$. Some flights have missing data. Also provided is the Spearman correlation coefficient, R, between each variable and $\Delta OA_{initial}$ and physical age for each variable. Note that panels (a), (d), and (g) have a log y-axis.

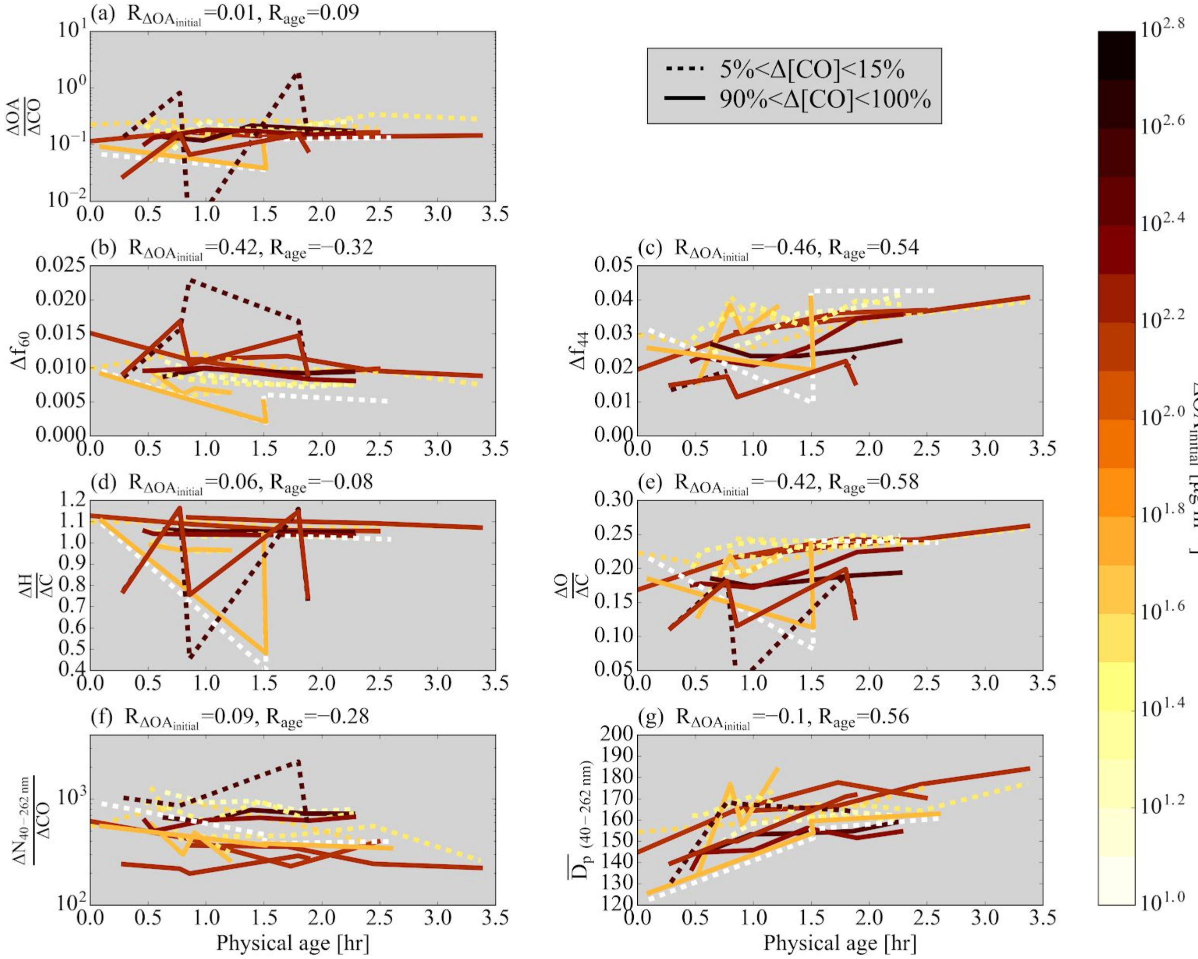

Figure S20. Various normalized parameters as a function of age for the 7 sets of pseudo-Lagrangian transects. Separate lines are shown for the edges (lowest 5-15% of ΔCO; dashed lines) and cores (highest 90-100% of ΔCO; solid lines). (a) ΔOA/ΔCO, (b) Δf_{60}, (c) Δf_{44}, (d) ΔH/ΔC, (e) ΔO/ΔC, (f) $\Delta N_{40\text{-}262\ nm}$/ΔCO, and (g) $\overline{D_p}$ between 40-262 nm against physical age for all flights, colored by $\Delta OA_{initial}$. Some flights have missing data. Also provided is the Spearman correlation coefficient, R, between each variable and $\Delta OA_{initial}$ and physical age for each variable. Note that panels (a), (d), and (g) have a log y-axis. This figure is identical to Figure 2 but uses an in-plume CO cutoff of 200 ppb.

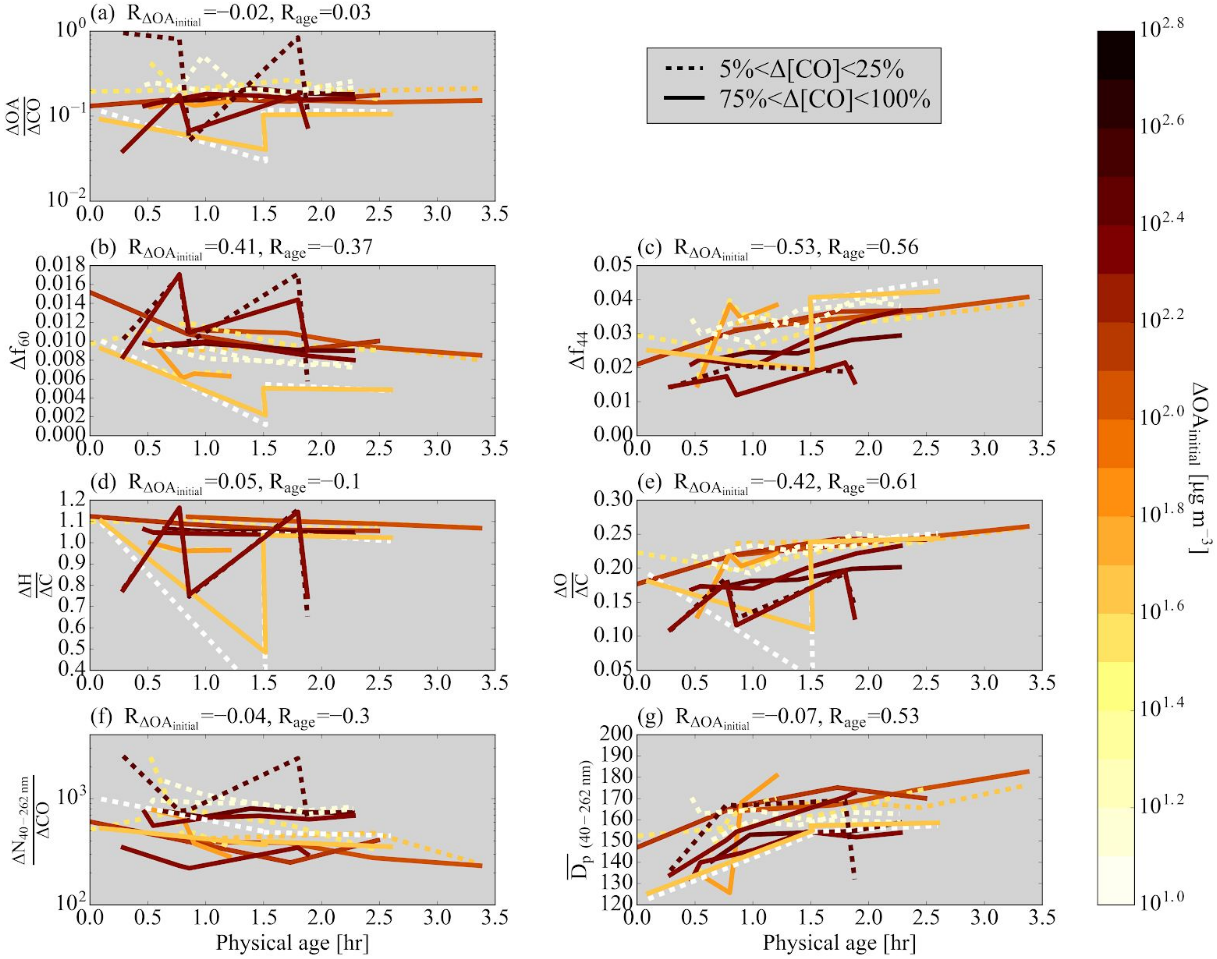

Figure S21. Various normalized parameters as a function of age for the 7 sets of pseudo-Lagrangian transects. Separate lines are shown for the edges (lowest 5-25% of ΔCO; dashed lines) and cores (highest 75-100% of ΔCO; solid lines). (a) ΔOA/ΔCO, (b) Δf_{60}, (c) Δf_{44}, (d) ΔH/ΔC, (e) ΔO/ΔC, (f) $\Delta N_{40\text{-}262\ nm}$/ΔCO, and (g) $\overline{D_p}$ between 40-262 nm against physical age for all flights, colored by $\Delta OA_{initial}$. Some flights have missing data. Also provided is the Spearman correlation coefficient, R, between each variable and $\Delta OA_{initial}$ and physical age for each variable. Note that panels (a), (d), and (g) have a log y-axis. This figure is identical to Figure 2 but uses different ΔCO percentile widths.

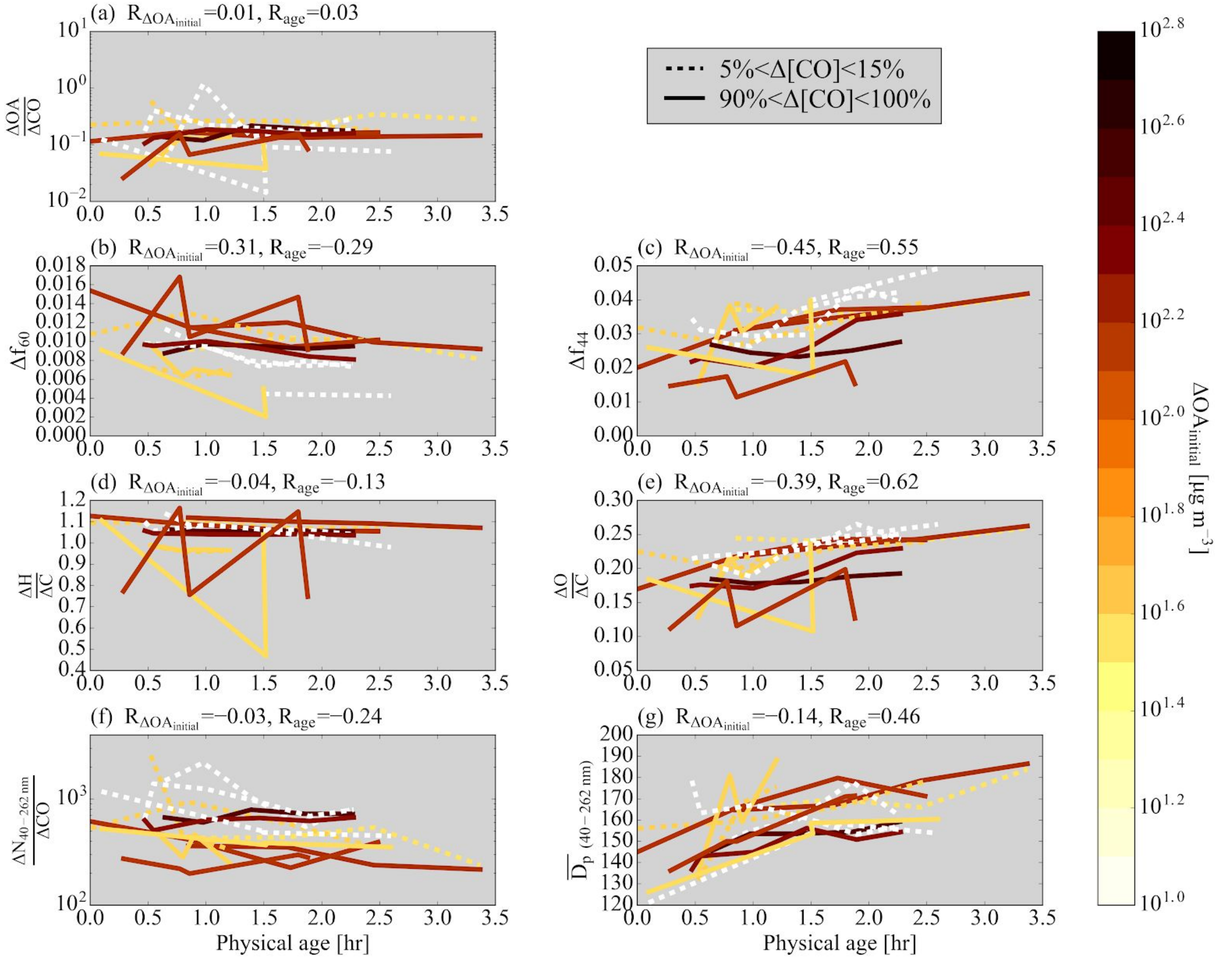

Figure S22. Various normalized parameters as a function of age for the 7 sets of pseudo-Lagrangian transects. Separate lines are shown for the edges (lowest 5-15% of ΔCO; dashed lines) and cores (highest 90-100% of ΔCO; solid lines). (a) ΔOA/ΔCO, (b) Δf_{60}, (c) Δf_{44}, (d) ΔH/ΔC, (e) ΔO/ΔC, (f) $\Delta N_{40\text{-}262\ nm}/\Delta CO$, and (g) $\overline{D_p}$ between 40-262 nm against physical age for all flights, colored by $\Delta OA_{initial}$. Some flights have missing data. Also provided is the Spearman correlation coefficient, R, between each variable and $\Delta OA_{initial}$ and physical age for each variable. Note that panels (a), (d), and (g) have a log y-axis. This figure is identical to Figure 2 except that it uses the location of the lowest 25% of CO data to determine the background concentrations of each species.

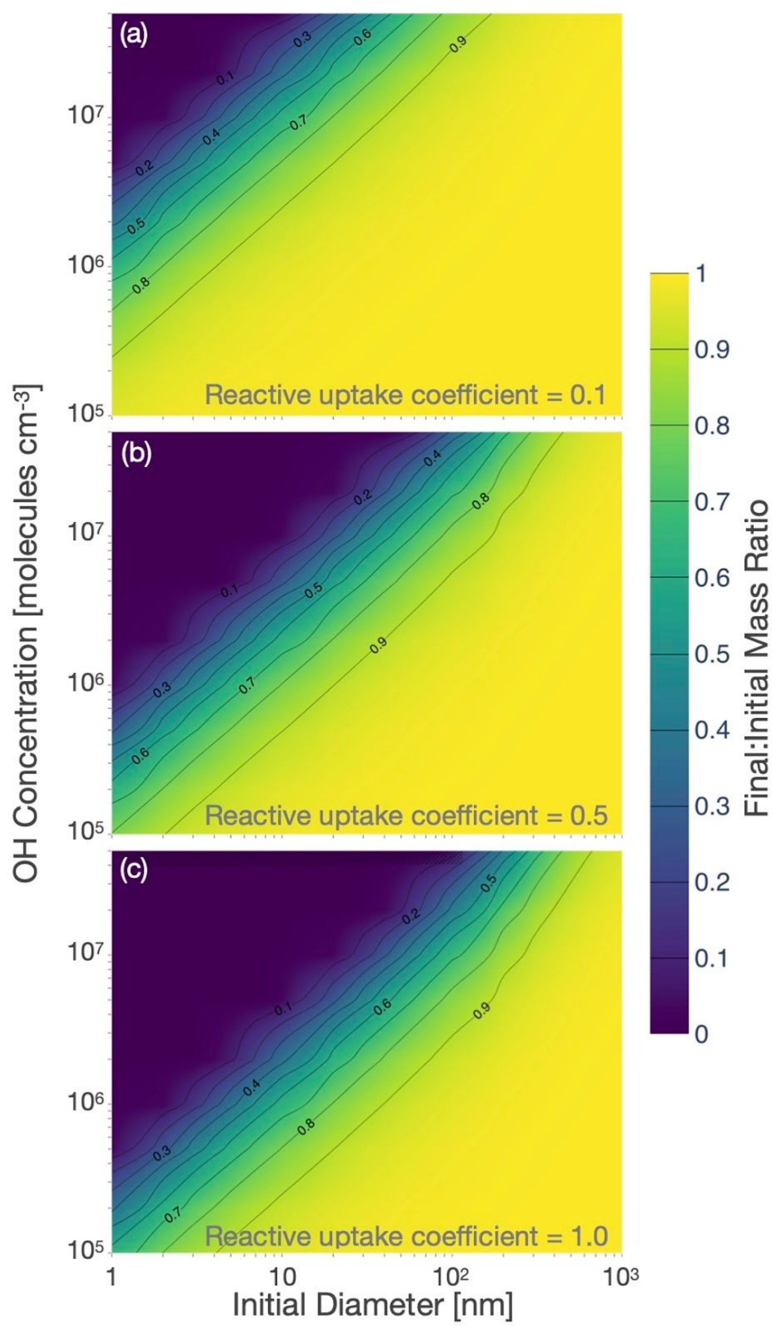

Figure S23. Calculated (final aerosol mass):(initial aerosol mass) ratios for mass loss through heterogeneous chemistry over a range of aerosol diameters and OH concentrations. As an upper-bound case, (a) it is assumed that for each OH collision, 200 amu of mass is lost. As a middle-bound, (b) it is assumed that 50% of OH collisions result in a 200 amu mass loss. As a more-realistic loss rate, (c) assumes that 10% of all OH collisions result in an 200 amu mass loss. See SI text S2 for more details.

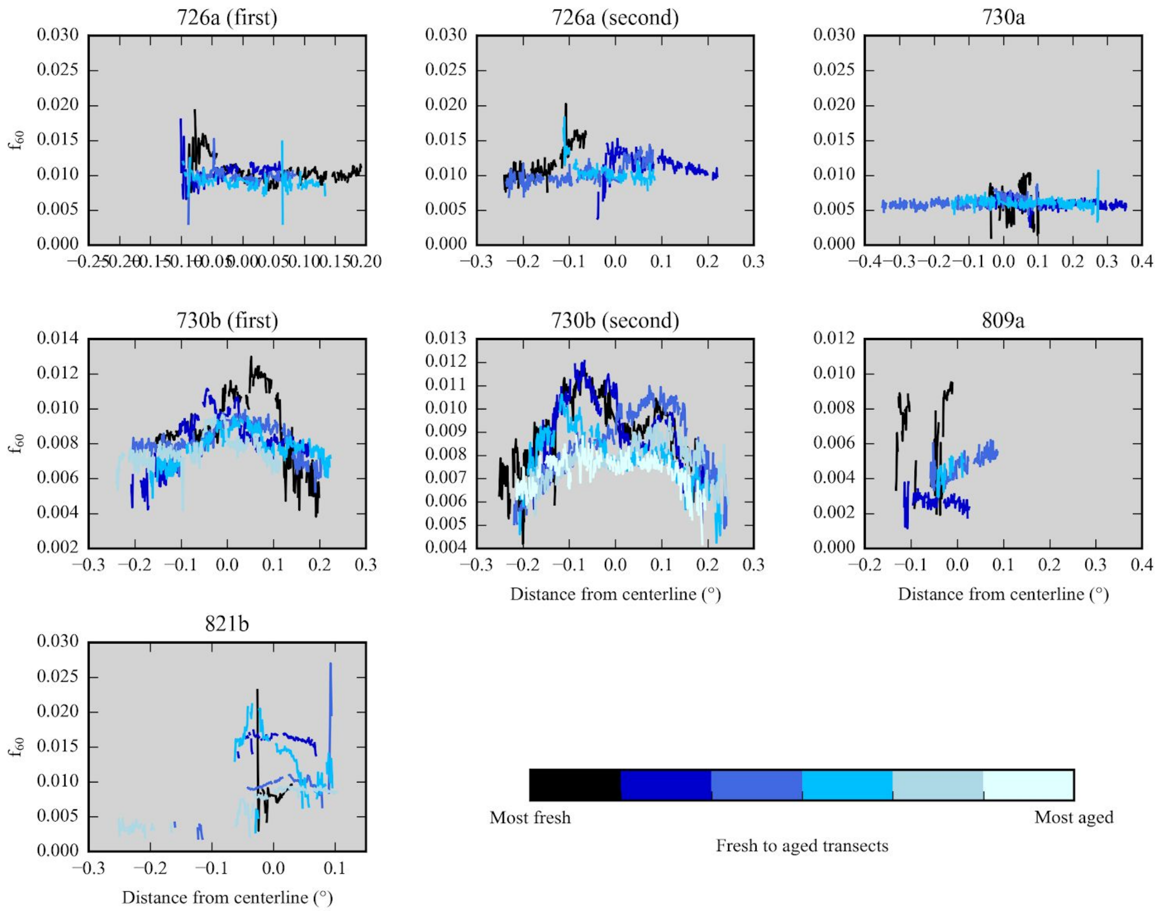

Figure S24. Raw f_{60} data for each flight along each transect included in this study. The titles indicate the flight. The black color indicates the earliest transect, with increasingly lighter colors indicating increasingly downwind transects. The centerline was estimated from the number size distribution and the estimated center of the fire (Figures S1-S6).

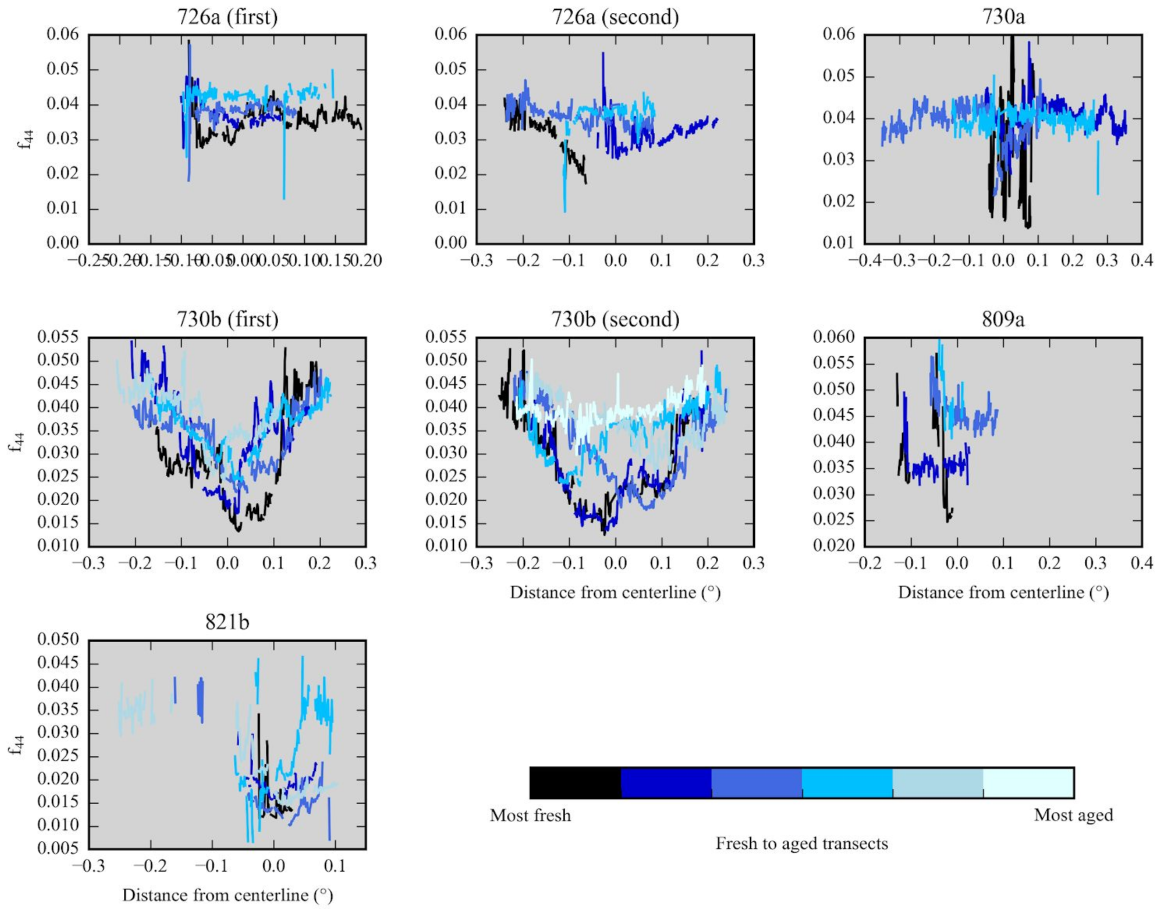

Figure S25. Raw f_{44} data for each flight along each transect included in this study. The titles indicate the flight. The black color indicates the earliest transect, with increasingly lighter colors indicating increasingly downwind transects. The centerline was estimated from the number size distribution and the estimated center of the fire (Figures S1-S6).

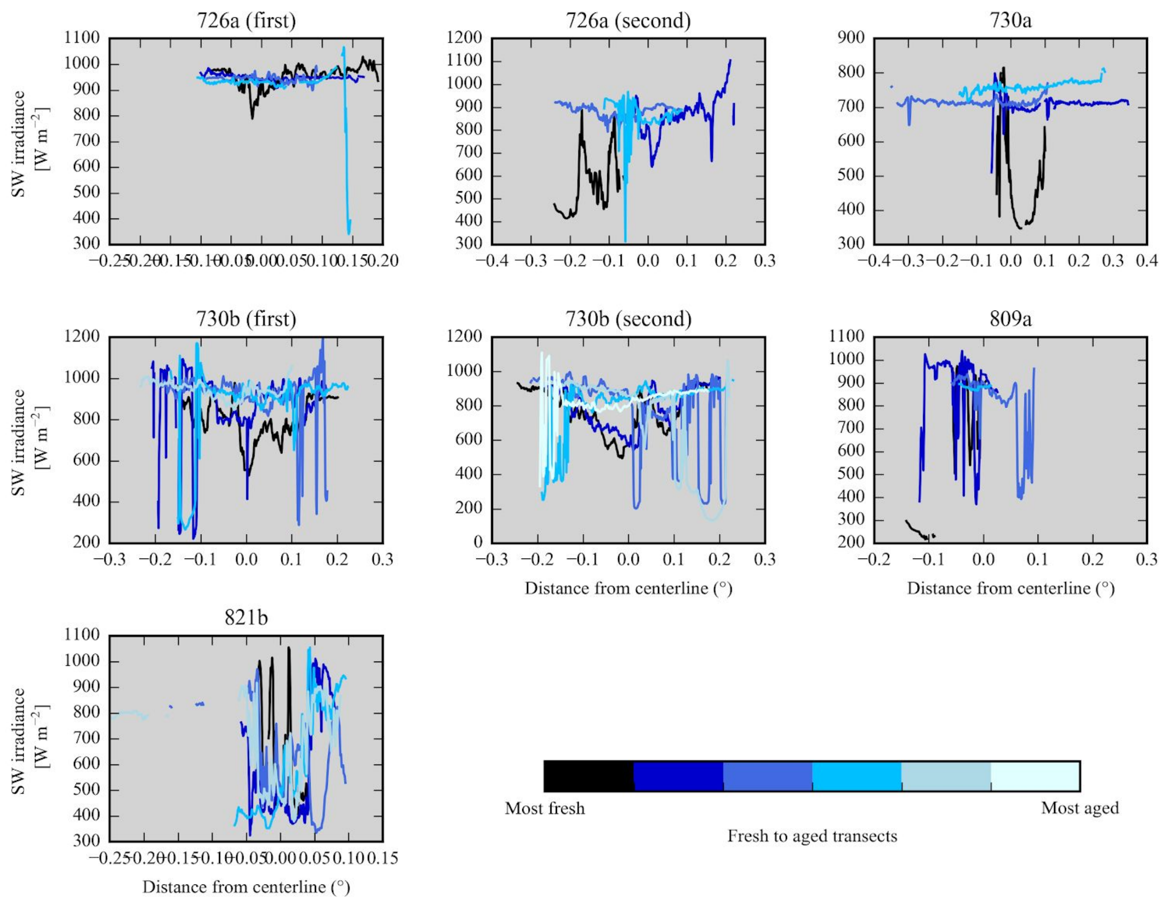

Figure S26. Total in-plume shortwave (SW) irradiance for each flight along each transect included in this study. The titles indicate the flight. The black color indicates the earliest transect, with increasingly lighter colors indicating increasingly downwind transects. The centerline was estimated from the number size distribution and the estimated center of the fire (Figures S1-S6).

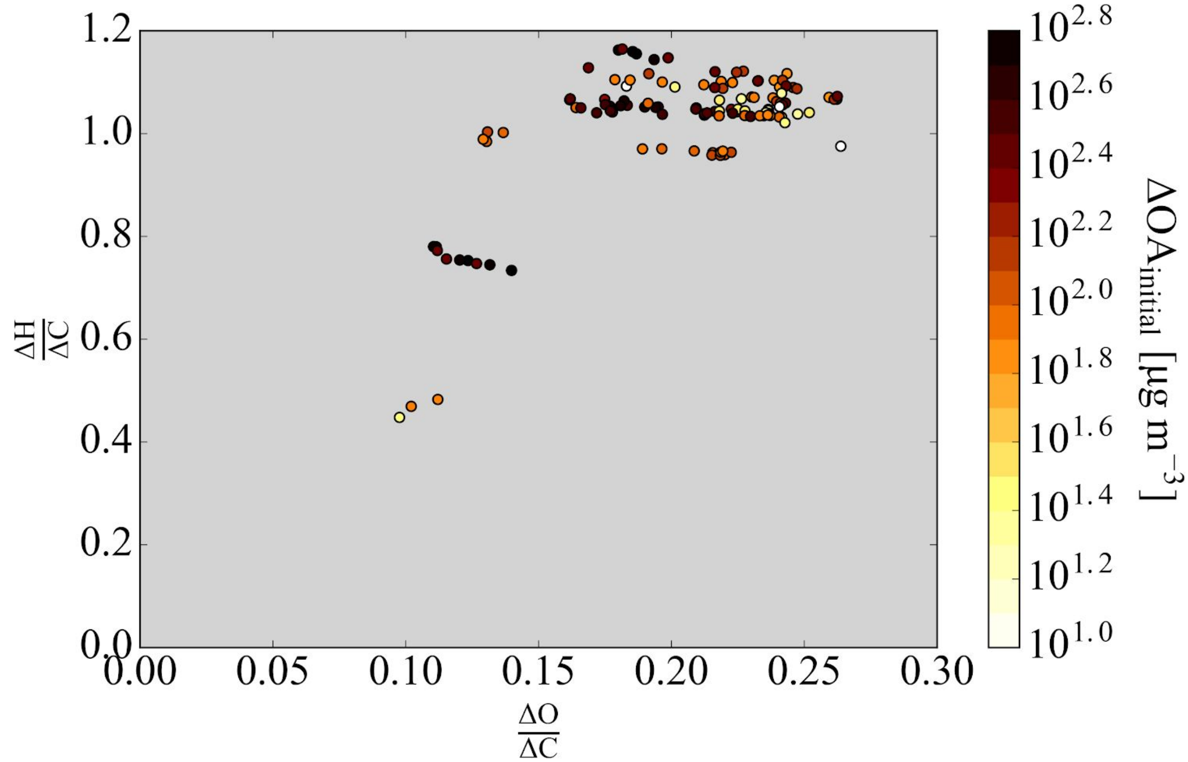

Figure S27. The Van Krevelen diagram of ΔH/ΔC versus ΔO/ΔC for all points in the 7 sets of pseudo-Lagrangian transects, colored by $\Delta OA_{initial}$.

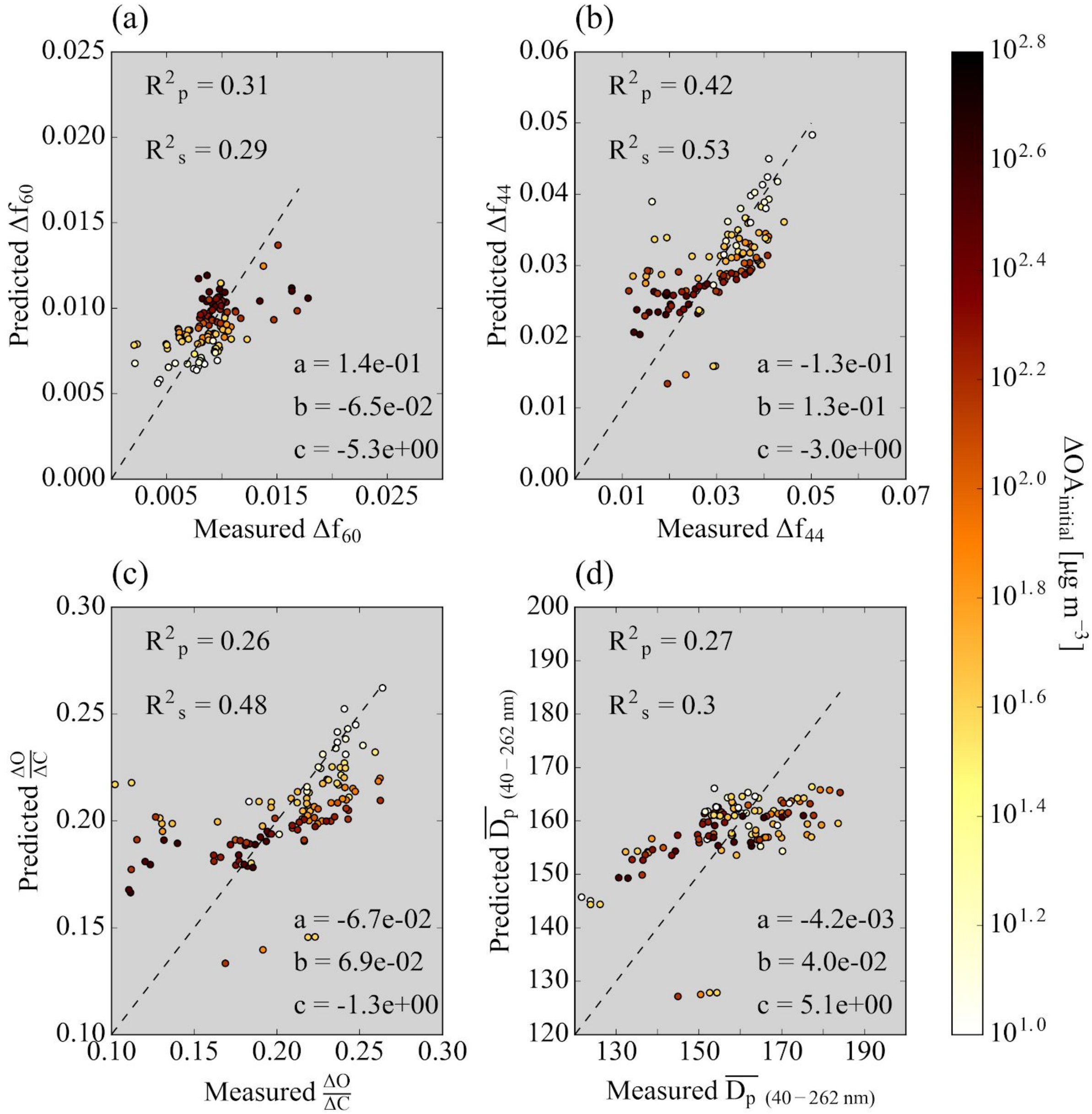

Figure S28. Measured versus predicted (a) Δf_{60}, (b) Δf_{44}, and (c) $\overline{D_p}$ between 40-262 nm, using the equation $ln(X) = a\ ln(\Delta OA_{initial}) + b\ ln(Physical\ age) + c$ where X=Δf_{60}, Δf_{44}, or $\overline{D_p}$. The values of *a, b,* and *c* when the equation is solved for *X* are provided within each subpanel, as are the Pearson and Spearman coefficients of determination (R^2_p and R^2_s, respectively). Included in the fit and figure are all four regions within the plume (the 5-15%, 15-50%, 50-90%, and 90-100% of ΔCO), all colored by the mean $\Delta OA_{initial}$ of each ΔCO percentile range.

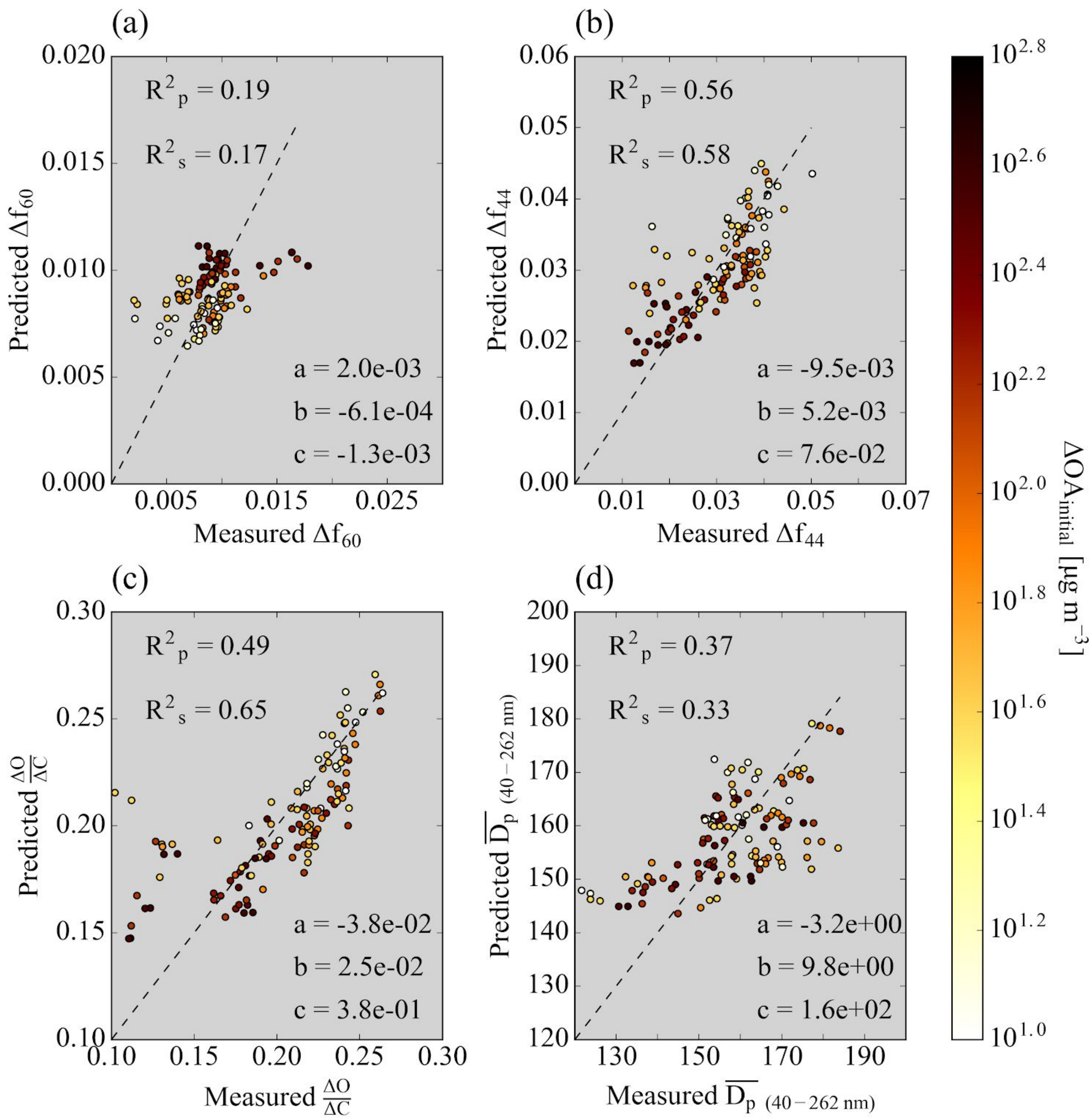

Figure S29. Measured versus predicted (a) Δf_{60}, (b) Δf_{44}, and (c) $\overline{D_p}$ between 40-300 nm, using the equation $X = a\ log_{10}(\Delta N_{\ initial}) + b\ (Physical\ age)\ + c$ where X=Δf_{60}, Δf_{44}, or $\overline{D_p}$ where X=Δf_{60}, Δf_{44}, or $\overline{D_p}$. Note that the fit here is the same as that in Eq. 2 except that $\Delta N_{initial}$ replaces $\Delta OA_{initial}$. The values of *a, b,* and *c* when the equation is solved for *X* are provided within each subpanel, as are the Pearson and Spearman coefficients of determination (R^2_p and R^2_s, respectively). Included in the fit and figure are all four regions within the plume (the 5-15%, 15-50%, 50-90%, and 90-100% of ΔCO), all colored by the mean $\Delta OA_{initial}$ of each ΔCO percentile range.